Materials Advances

ROYAL SOCIETY OF CHEMISTRY

PAPER

View Article Online
View Journal | View Issue

Cite this: *Mater. Adv.*, 2025, **6**, 1635

Study of the electrochemical performance of *Zanthoxylum armatum* seed-derived potassium hydroxide-assisted activated carbon as a negatrode material for supercapacitor applications

Deval Prasad Bhattarai,[a] Sabin Aryal,[a] Khem Raj Shrestha,[b] Pawan Kumar Mishra,[c] Timila Shrestha,[a] Puspa Lal Homagai,[a] Hari Bhakta Oli *[a] and Ram Lal (Swagat) Shrestha*[a]

Received 27th September 2024,
Accepted 23rd January 2025

DOI: 10.1039/d4ma00980k

rsc.li/materials-advances

With the rampant increase of the wearable electronics domain, there is an urgent need for the development of sustainable, cost-effective, and durable energy storage devices utilizing bio-waste materials. Supercapacitors are the promising energy storage solution among the various energy storage devices. In this work, *Zanthoxylum armatum* seed-based activated carbon has been prepared by precarbonization at 280 °C followed by potassium hydroxide (KOH)-assisted carbonization at 900 °C under a nitrogen atmosphere. The as-prepared activated carbon was tested with various physicochemical and electrochemical techniques to assess its suitability as a negative electrode for supercapacitor applications. The Brunauer–Emmett–Teller (BET) surface analysis revealed that the KOH-activated *Z. armatum* (KZAC) carbon material exhibited a specific surface area of 554.10 $m^2\ g^{-1}$. The results show 148.08 F g^{-1} specific capacitance at 0.5 A g^{-1} current density with excellent capacitance retention, making it a promising material for negative electrode fabrication.

1. Introduction

In the era of research and scientific innovation, researchers are focused on solving the formidable challenge of addressing the escalating global energy demand in tandem with rapid population growth and lethal environmental effects of fossil fuel exploitation.[1] At this moment, electrochemical energy storage systems like supercapacitors, batteries, capacitors, *etc.* are in the forefront to meet the energy requirement of this time.[2] Being environmentally friendly and low-cost materials which can provide a burst of power in a fraction of second, supercapacitors, also known as electrochemical capacitors, are highly favorable energy storage systems.[3] In addition, the exceptional power density, rapid energy delivery, extended cycle life with excellent stability, and wide range of operational temperatures make it an ideal choice. Based on the charge storage mechanism, supercapacitors are classified into electric double-layer supercapacitors (EDLCs) and pseudocapacitors.[4–6] Among these, the EDLC-type of supercapacitors store energy by physical separation of the charge in the electric double layer by pure electrostatic interactions allowing near-instantaneous charge and discharge processes. This is in stark contrast to the conventional batteries as the latter relies on slower chemical reactions to store and release energy.[7] Compared to batteries, supercapacitors do not suffer from depth of discharge limitations and fully utilize the stored energy without conceding life expectancy. On the one hand, the high coulombic efficiency of the EDLCs minimizes the energy loss during charge–discharge cycles and on the other hand the absence of chemical reaction attenuates the thermal runaway enhancing the safety.[8] All in all, these properties underscore the benefits of establishing supercapacitors as an ideal energy storage system.

The electrochemical performance of supercapacitors fabricated from naturally derived materials augments critical consideration in terms of affordability.[9] In this context, carbonaceous materials like activated carbon, graphene, metal organic frameworks, *etc.* have garnered considerable attention in the supercapacitor field. Waste materials can be valorized to attain active carbonaceous materials as low-cost or no-cost

[a] *Department of Chemistry, Amrit Campus, Tribhuvan University, Kathmandu, Nepal. E-mail: hari.oli@ac.tu.edu.np, swagatstha@gmail.com*
[b] *Nanomaterials lab, Department of Applied Sciences and Chemical Engineering, Pulchowk Campus, Tribhuvan University, Kathmandu, Nepal*
[c] *Department of Chemistry, Tri-Chandra Multiple Campus, Tribhuvan University, Kathmandu, Nepal*

materials for the preparation of electrode materials.[10] Due to their environmental friendliness, sustainability, and cost-effectiveness profiles, activated carbon derived from bio-waste is at the frontline in the realm of supercapacitors.[11] In this context, the utilization of bio-waste materials for the production of activated carbon primarily has two benefits: (i) bio-waste is the best alternative source for the production of AC as it uses sustainable and renewable sources of bio-waste materials rather than non-renewable fossil sources, which helps in minimization of the waste in the environment. (ii) Pore size can be customized and tailored to get enhanced electrochemical performance.[12] The exceptional properties of the activated carbon encompass the enhanced electrochemical properties along with the lightweight nature, adjustable pore size, and capacious surface area. Activated carbon can be synthesized using various biomasses sources like coconut shells, litchi seeds, orange peels, rice husks, banana peels, and many more. These are glorified for their environmental sustainability and their contribution in long-term energy storage solutions.[13]

Even though the process of synthesis of the activated carbon utilizing biomass sources is facile, it is fraught with numerous challenges. The presence of impurities or contaminants in the activated carbon can hinder the performance of electrode materials and heterogeneity in the chemical composition.[14] Additionally, tuning the porous structure of carbonaceous materials by the rational selection of precursor materials, the route of activation and choice of activating agent with optimized impregnation ratio in the realm of environmental consideration is a critical issue in the preparation of biomass-based activated carbon.[15] Both the activation processes, physical as well as chemical activation, involve the removal of the volatile organic matter from the biomass generating micropores, mesopores, and macropores.[16] The action of the activating agent to the lignocellulosic materials constituent in the biomass plays a crucial role in the porosity and surface area of the activated carbon. Each of the chemical activating agents like KOH, $ZnCl_2$, H_3PO_4, H_2SO_4, *etc.* has its own distinctive properties, which is imperative to generate minute pores with variation.[16–19] The architectonics of the generated pores is vital for the large specific surface area, which in turn contributes to the higher specific capacitance aiding ion transport.[20]

KOH interacts with carbonaceous materials through dehydration and decarboxylation processes, eliminating volatile components and forming a porous structure.[21,22] They reduce the activation energy for the breakdown of organic materials enhancing the rate of carbonization, and activation. At elevated temperature, the potassium compound gets reduced to metallic potassium and it can stimulate the intercalation of the potassium into the carbon matrix prompting the separation of the carbon layers, consequently forming micropores and mesopores. During high temperature treatment, KOH reacts with the lignocellulosic materials present in the biomass and results in the production of hydrogen gas along with potassium carbonate (K_2CO_3).[23] The evolution of the gas is beneficial as it traces out new pores in the carbon structure. The treatment of KOH introduces functional groups such as carboxylates, lactones, and phenolates on the surface of the active materials, which contributes to altering the surface reaction.[24]

In this work, porous activated carbon was generated utilizing the waste seeds of *Z. armatum* DC. The chemical activation followed by physical activation of its seeds, *i.e.*, carbonization of the impregnated materials produces highly porous activated carbon. An extensive literature review shows that the potentiality of *Z. armatum* seed-derived activated carbon as a supercapacitor material has yet to be explored. Based on this background, *Z. armatum* seed powder was impregnated with KOH and subjected to a carbonization process at 900 °C under a nitrogen atmosphere, which exhibited BET surface area of 554.10 $m^2\ g^{-1}$. The electrochemical performance of the as-prepared activated carbon was studied in terms of cyclic voltammetry (CV), electrochemical impedance spectroscopy (EIS) and galvanostatic charge discharge (GCD). The results show 148.0 F g^{-1} specific capacitance at 0.5 A g^{-1} current density. It shows that the AC can be a promising material for negative electrode fabrication.

2. Experimental section

2.1. Chemical reagents

Potassium hydroxide (KOH, mol. wt. 56.11, purity ≥ 85%, NIKE), hydrochloric acid (HCl, Mol. Wt. 36.46, Fischer Scientific, purity 35–37%), ethanol, polyvinylidene fluoride (PVDF), propan-2-ol, and Ni-foam were used in this work. All the chemicals were of analytical grade and were used as-received without further purification.

2.2. Process of synthesis

2.2.1. Sample collection and preparation. The seeds of *Z. armatum* DC were collected from Palung, Makawanpur district, Nepal. They were isolated and subjected to desiccation at 80 °C for 18 h. Subsequently, the material was milled into a fine powder utilizing an herbal medicine disintegrator (FW177). This powder was further dried at 100 °C for 3 h in a standard laboratory oven.

2.2.2. Preparation of porous activated carbon. The dried powder of *Z. armatum* was subjected to heating at 280 °C for 4 h in a muffle furnace; resulting in what is hereafter referred to as pre-carbonized materials. It was then impregnated with chemical activator potassium hydroxide (KOH) in a 1 : 1 mass ratio with thorough mixing. It was homogenized by meticulously grinding for about 3 h using an agate mortar and pestle. The homogenized mixture was then subjected to carbonization at 900 °C under a nitrogen atmosphere. The temperature was increased at a ramp of 5 °C min^{-1}. The carbonization was conducted in a tube furnace (KJ-T1200 Tube Furnace, Zhengzhou Kejia Furnace Co. Ltd, China) under an inert nitrogen atmosphere at the flow rate of 120 cc min^{-1} for 3 h. The KOH impregnated material carbonized at 900 °C is labelled as KZAC. After that, the carbonized samples were powdered thoroughly in an agate mortar using a pestle. The homogenized KZAC sample was then transferred to a 250 mL beaker and gradually

treated with 1 M hydrochloric acid (HCl). To the solution, 150 mL deionized water was added and continuously stirred for 30 minutes. Then it was allowed to settle for 1 hour for decantation. The supernatant solution was carefully decanted, and the residual solid was repeatedly washed with distilled water until neutral pH was achieved. The neutralized final product was vacuum dried at 80 °C for 12 h and it was further ground one more time and stored in a desiccator for subsequent characterization and analyses.

2.2.3. Physicochemical characterization. The X-ray diffraction (XRD) patterns of the as prepared samples in powdered form were obtained by using a Rigaku Diffractometer with CuKα radiation (wavelength λ = 1.54059 Å) at an operating voltage of 40 kV and current of 40 mA. The scanning rate was set at 2.5° min^{-1}, covering a range of 5–80° at room temperature. The presence of surface functional groups in the activated carbon samples was ensured by Fourier transform infrared (FTIR) spectroscopy using a PerkinElmer Spectrum IR Version 10.6.2 operating in attenuated total reflection (ATR) mode, covering the range of 4000 cm^{-1} to 400 cm^{-1} at room temperature. The surface morphology of the activated carbon was examined using a field emission scanning electron microscope (FESEM) (JEOL, JSM-6701F, Tokyo, Japan). Additionally, energy dispersive X-ray (EDX) analysis was performed using FESEM to quantify the elemental composition and distribution within the samples.

The specific surface areas of the synthesized activated carbon samples were determined through Brunauer–Emmett–Teller (BET) analysis, while the pore size distribution was assessed using the Barrett–Joyner–Halenda (BJH) technique with Quantachrome Instruments software (v11.05). The specific surface area was calculated *via* nitrogen adsorption/desorption measurements conducted within a relative pressure range of 0 to 1 Pascal at a temperature of 77 K. The BET equation used for this calculation is represented in eqn (1).

$$\frac{P}{V(P_0 - P)} = \frac{C - 1}{V_m C} \times \frac{P}{P_0} + \frac{1}{V_m C} \quad (1)$$

Here 'V' denotes the volume of nitrogen gas adsorbed, 'V_m' represents volume of N_2 gas adsorbed to form a monolayer at standard temperature and pressure (STP), 'C' is a constant term related to the adsorbate's enthalpy, 'P_0' is the saturated vapour pressure and 'P' is the partial vapor pressure of the gas at equilibrium at 77.3 K, respectively.

2.2.4. Electrochemical characterization. The electrochemical analysis, *i.e.* cyclic voltammetry (CV), galvanostatic charge discharge (GCD), and electrochemical impedance spectroscopy (EIS) were performed using a CorrTest Electrochemical workstation (CS 350, Wuhan Corrtest Instruments Corp., Ltd). The electrochemical tests were performed in a three-electrode system, with the active material deposited onto nickel foam by the drop casting method. A mercury/mercury oxide (Hg/HgO) electrode in 6 M KOH solution served as the reference electrode, and a platinum electrode was used as the counter electrode.

While preparing the working electrode, a slurry was prepared by dissolving 10% polyvinylidene fluoride (PVDF) in propan-2-ol solvent. The active sample, carbon black, and polyvinylidene fluoride (PVDF) were mixed in a ratio of 8 : 1 : 1 with the requisite amounts of propan-2-ol and the content was ground using a mortar and pestle. After homogenizing the slurry, it was drop cast onto a nickel foam substrate (1 × 1 cm^2) and dried at 60 °C for 12 h. The activated carbon loaded Ni-foam had an active mass of 4 mg cm^{-2} and acts as the working electrode for the electrochemical analysis. The CV and GCD data were obtained within the potential window of −1.0 to 0.0 V at different scan rates. For the analysis of the electrochemical impedance, a Nyquist plot was used at the frequencies of 100 kHz to 1 mHz. The specific capacitance of the electrode material was calculated from the galvanostatic charge–discharge curve using eqn (2).

$$C_{sp} = \frac{I \times \Delta t}{m \times \Delta v} \quad (2)$$

where I is the charge–discharge current in ampere (A), Δt is the discharge time in seconds, m is the active mass of activated carbon loaded on Ni-foam in grams (g), and Δv is the potential window in volts.

3. Results and discussion

3.1. Physicochemical characterization

The waste part of *Z. armatum* seed was separated from the edible part and it was ground into a fine powder, which was then subjected to heat treatment in a muffle furnace at 280 °C for 4 h; allowing it to cool naturally. as the as-obtained sample before the carbonization process is termed as pre-carbonized *Z. armatum* char (PCZ). The dried pre-carbonized materials were then impregnated with potassium hydroxide (KOH) in 1 : 1 mass ratio and allowed to mature for 24 h. After that, the impregnated sample was subjected to carbonization at 900 °C, under an inert nitrogen atmosphere for 3 h. It was supposed that the carbonization procedure removes volatile organic matter due to the combined action of the activating agent and the heat treatment. The yield of activated carbon obtained after carbonization of PCZ was calculated by using the following relation (3).

$$\text{Yield } (\%) = \frac{\text{Mass of the activated sample } (W_{AC})}{\text{Mass of impregnated sample } (W_0)} \times 100\% \quad (3)$$

A yield of 9.8% was achieved from 5 g of PCZ after activation with KOH at 900 °C for 3 h under a nitrogen atmosphere.

During the carbonization process at 900 °C under a nitrogen atmosphere, complex reactions take place between the activating agent and the carbon rich lignocellulosic materials confiscating volatile matters in the form of gases like CO_2, CO, *etc.* leaving behind a highly porous 3D structure. The nature and action of the activating agent toward the carbonaceous materials is crucial in obtaining hierarchical porous carbon with excellent quality. During the period of activation, pyrolysis using potassium hydroxide at 900 °C, the activating agent KOH first reacts with active oxygen-rich species like C═O, –OH, C–O, O–C═O, and –COOH groups present in the sample resulting into the destruction of oxygen containing moieties with the

release of a large amount of respective free radicals creating a number of vacancies in the carbon structure. In the meantime, a fraction of the KOH reacts with C–C and C–H groups and etched the carbon fragment with releasing hydrogen to generate vacancies. These vacancies are occupied by the –OH group (from KOH) and numerous new oxygen-containing groups are produced in the biochar. Potassium carbonate (K_2CO_3) could be formed at 400–700 °C by the reaction of KOH and oxygen-containing carbon materials. At 800 °C, it gets further transformed into K_2O. At this point, metallic potassium (K) along with gaseous products are produced.

$$K_2CO_3 \rightarrow K_2O + CO_2$$

$$2K + CO_2 \rightarrow K_2O + CO$$

$$K_2O + H_2 \rightarrow 2K + H_2O$$

$$K_2O + C \rightarrow 2K + CO$$

It is presumed that the metallic potassium produced during the activation process gets penetrated into the internal structure of the carbon matrix expanding the existing pores along with creating new pores.[25] In addition, it is believed that it catalyzes the activation process to some extent enhancing the degree of graphitization. These processes promote the oxygen content and porosity of the carbon materials.[26]

Physicochemical characterization. At elevated temperature, the carbon materials were graphitized with enhanced density of the electrons/holes/ions which take part in the electrical conductivity and enhanced electron mobility along with the finite probability of transmission of charge carrier species.

The crystallinity and phase homogeneity of the KOH activated carbon (KZAC) and precarbonized *Z.* char from the waste part of the *Z. armatum* seeds were assessed by powder X-ray diffraction (PXRD) analysis, as shown in Fig. 1(a). The prominent XRD patterns at around 23.5° two theta value with a *d*-spacing of 3.628 Å correspond to the (002) plane and peak of 43.17° two theta value with *d*-spacing 2.068 Å correspond to the (001) plane. Furthermore, the PXRD patterns of the sample under the exploration unveil characteristics of an amorphous structural state. The FTIR spectra reveal a transmittance band of –OH groups at around 3400 cm^{-1}, $-CH_2$ stretching at around 2915 cm^{-1} and carbonyl groups at around 1720 cm^{-1}, which are diminished upon carbonization. It shows the carbonization of the sample.

The specific surface area of the as prepared activated carbon was analyzed by the Brunauer–Emmett–Teller (BET) surface measurement method *via* adsorption–desorption isotherms of nitrogen at −196 °C and the Barrett–Joyner–Halenda (BJH) method was applied to assess the pore size distribution of the KZAC and PCZ samples. The BET isotherms and BJH plots are depicted in Fig. 2(a–d). The KZAC sample exhibited a higher surface area of 554.101 $m^2\ g^{-1}$ exceeding that of PCZ (7.561 $m^2\ g^{-1}$). The BET isotherm of the KZAC showed the characteristic hysteresis loop of the type IV isotherm revealing a mesoporous structure with a noteworthy micropore area (137.146 $m^2\ g^{-1}$) and micropore volume (0.056 cc g^{-1}), confirming the material's nanoporous architecture. In contrast, PCZ demonstrated a Type II isotherm with minimal hysteresis, signifying a non-porous or macroporous structure with insignificant micropore volume (0.007 cc g^{-1}) with a micropore area of 4.844 $m^2\ g^{-1}$. This sample demonstrates a predominantly non-porous or macroporous structure. Due to the thermal treatment at elevated temperature of 900 °C facilitated by KOH activation, it results in an enhanced hierarchical nanoporous structure of KZAC. The superior surface area and mesoporosity of KZAC made it particularly well-suited for supercapacitor applications, owing to its improved diffusion properties.

The FESEM image of *Z. armatum* derived precarbonized carbon and *Z. armatum* derived activated carbon at 900 °C is shown in Fig. 3. The image shows the increased porosity upon

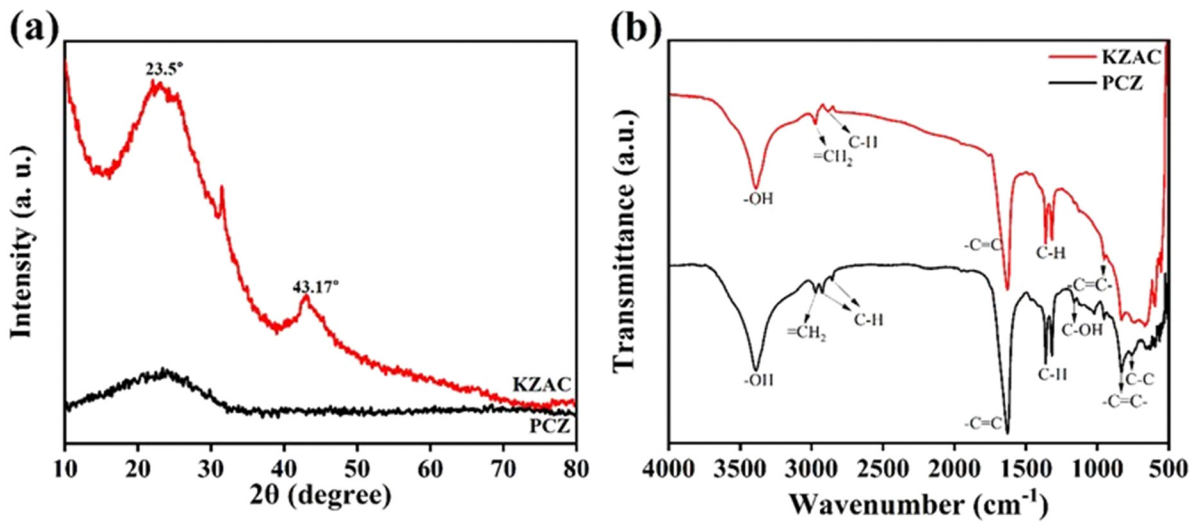

Fig. 1 (a) XRD and (b) FTIR of KZAC and PCZ.

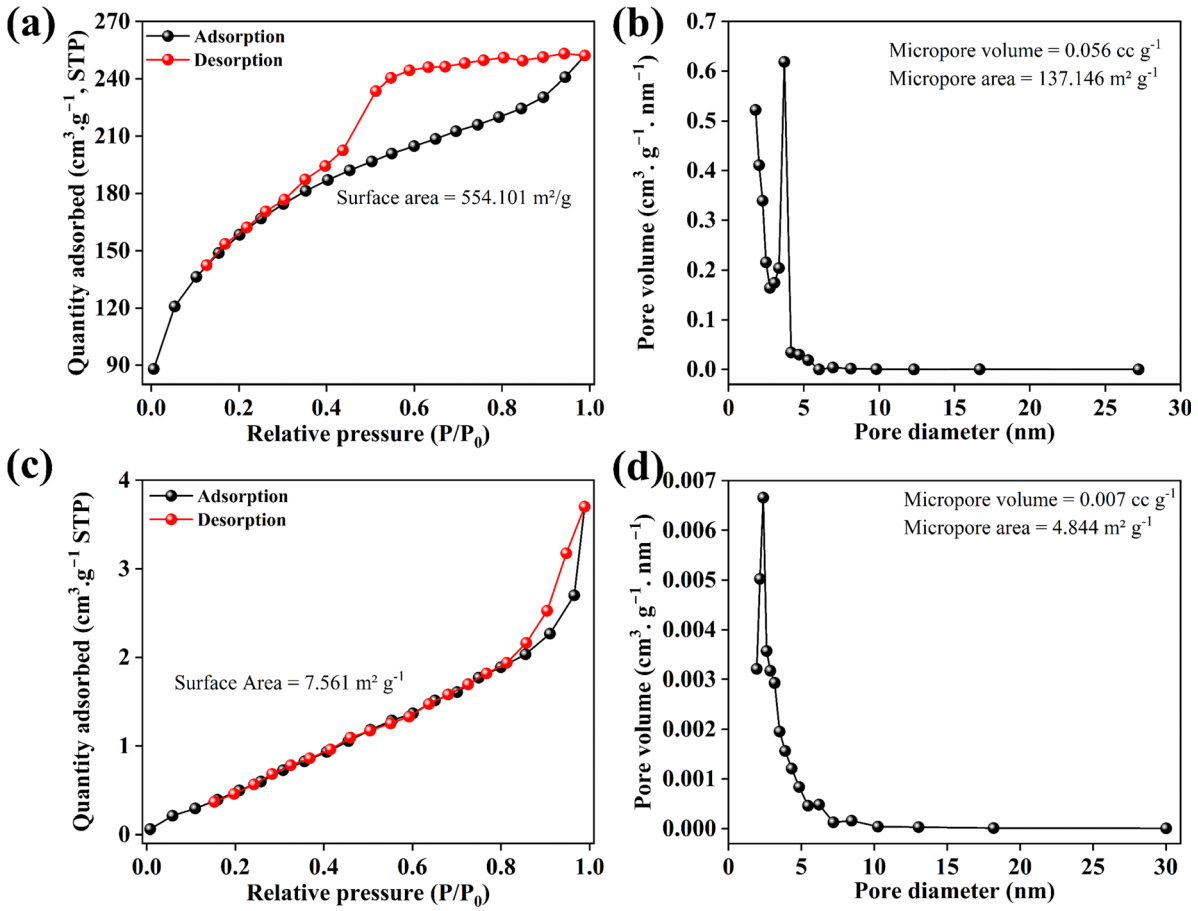

Fig. 2 BET analysis: (a) and (c) demonstrate N_2 adsorption–desorption isotherms, and (b) and (d) BJH pore size distribution of KZAC and PZC, respectively.

carbonization. In the precarbonization process, the powder biomass of *Z. armatum* seed was heated under ambient oxygen atmosphere at 280 °C for 4 h. During this period, volatile components were removed with the partial carbonization of lignocellulosic biomass. This results in the low porosity of the materials (Fig. 3(a)–(c)). When the same sample was carbonized at high temperature (900 °C), affluent carbonization of the material occurred with the release of effluent gas by carbonization. This results in the production of a hierarchical porous structure, which would be useful for the passage of ions into the channels in the electrochemical performance.

In addition, elemental mapping and energy dispersive X-ray spectroscopy were carried out for the sample (Fig. 4). EDX mapping shows the presence of C, N, O, Mg, K, and Ca in the precarbonized sample. The carbonized sample exhibited the presence of only C, N and O. It can be revealed from the fact that elements such as Mg, K and Ca are lost during the carbonization process. Most presumably, these elements are lost in the form of volatile vapor and ashes during the process of carbonization. The elemental color mapping for each element present in the pre-carbonized sample is depicted in Fig. 4.

The elemental color mapping for each element present in the KOH-activated *Z. armatum* derived activated carbon sample is depicted in Fig. 5.

3.2. Electrochemical characterization

The feasibility of the electrode materials for supercapacitor applications was assessed in terms of electrochemical analysis. The electrochemical behaviour of the KZAC was quantitatively evaluated within a 6 M KOH electrolyte using a three-electrode cell configuration. The cyclic voltammetry (CV) profiles for the sample under examination revealed a quasi-rectangular form indicating capacitive behavior of these materials (Fig. 6a). The CV measurements were conducted across a potential range extending from −1.0 to 0.0 V. Typically, carbon materials are used as the negatrode in supercapacitor applications. The CV plot of KZAC demonstrated a nearly rectangular shape, the typical characteristic of electric double-layer capacitor (EDLC) behavior.

Fig. 6(a) indicates that there is a consistent trend of increasing current response with the increase of scan rate (from 1 to 100 mV s^{-1}). This is in accordance with the empirical relation, $i = a\nu^b$, where, i is current, ν is sweep rate (scan rate in mV s^{-1}) and a is an adjustable parameter. The value of b indicates whether the process is a diffusion controlled or surface-controlled process. Qualitatively, the increase in current with increasing scan rate can be attributed to the limited time available for charge dissipation at higher scan rates. This results in the accumulation of charges at the electrode–electrolyte

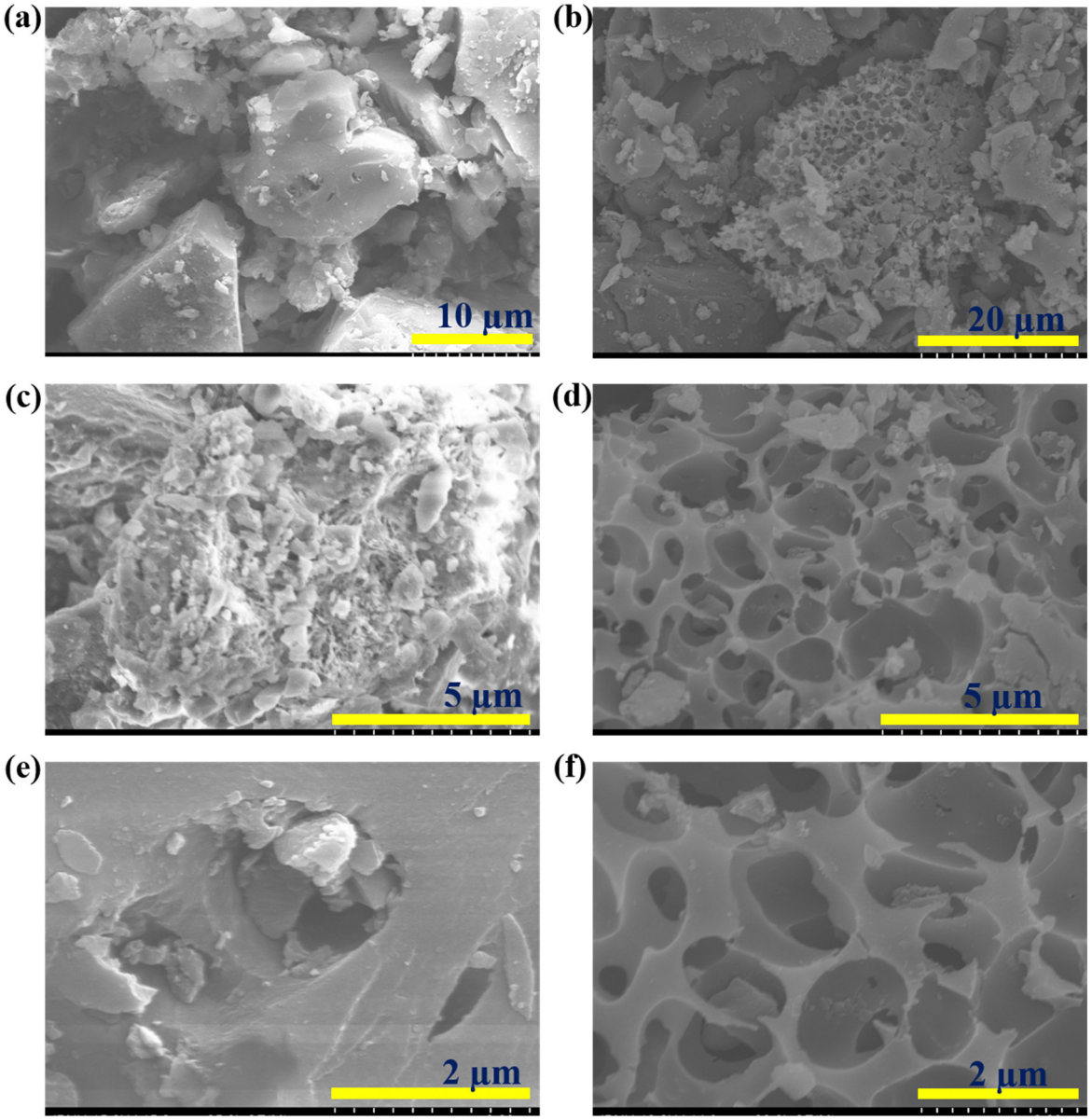

Fig. 3 Surface morphology study: FESEM image of (a), (c), (e) pre-carbonized *Z. armatum* derived carbon and (b), (d), (f) *Z. armatum* derived activated carbon under different magnification.

interface and subsequently increases the current and capacitance values.

The specific capacitance of the materials is computed using galvanostatic charge discharge (GCD) in a three-electrode configuration with current density ranging from 0.5 A g^{-1} to 20 A g^{-1} (Fig. 6b). Since the working electrode is solely made up of carbon materials, it showed a symmetrically linear charging–discharging curve, devoid of any redox peaks.

The sample KZAC displayed specific capacitance of 148.0, 100.3, 76.6, 61.8, 52.8, 46.5, 44, 43.5, and 26.0 F g^{-1} at a current density of 0.5, 1, 2, 3, 4, 5, 10, 15, and 20 A g^{-1}, respectively. The decrease in specific capacitance with increasing current density can be primarily attributed to factors like limitations in ion diffusion, restricted access of the electrolyte to the electrode surface, resistance effects, and electrode polarization. All these factors contribute to the effective charge storage capacity of the supercapacitor at higher current densities. The decrease in the capacitance is also associated with the IR drop, which is due to the internal resistance that causes some voltage to overcome the resistance of the system. KZAC exhibits better rate capability ~43% at a current density of 15 A g^{-1}. The better capability can be attributed to the 3D mesoporous architectonics of the activated carbon with higher surface area, which is derived using KOH.

The electron transfer kinetics of electrode was investigated by electrochemical impedance spectroscopy (EIS). The Nyquist plot was obtained in the frequency range of 100 kHz to 1 mHz with superimposing AC signal of amplitude ±10 mV. The Nyquist plot for the sample is presented in Fig. 6(c). From the Nyquist plot, different types of information can be obtained;

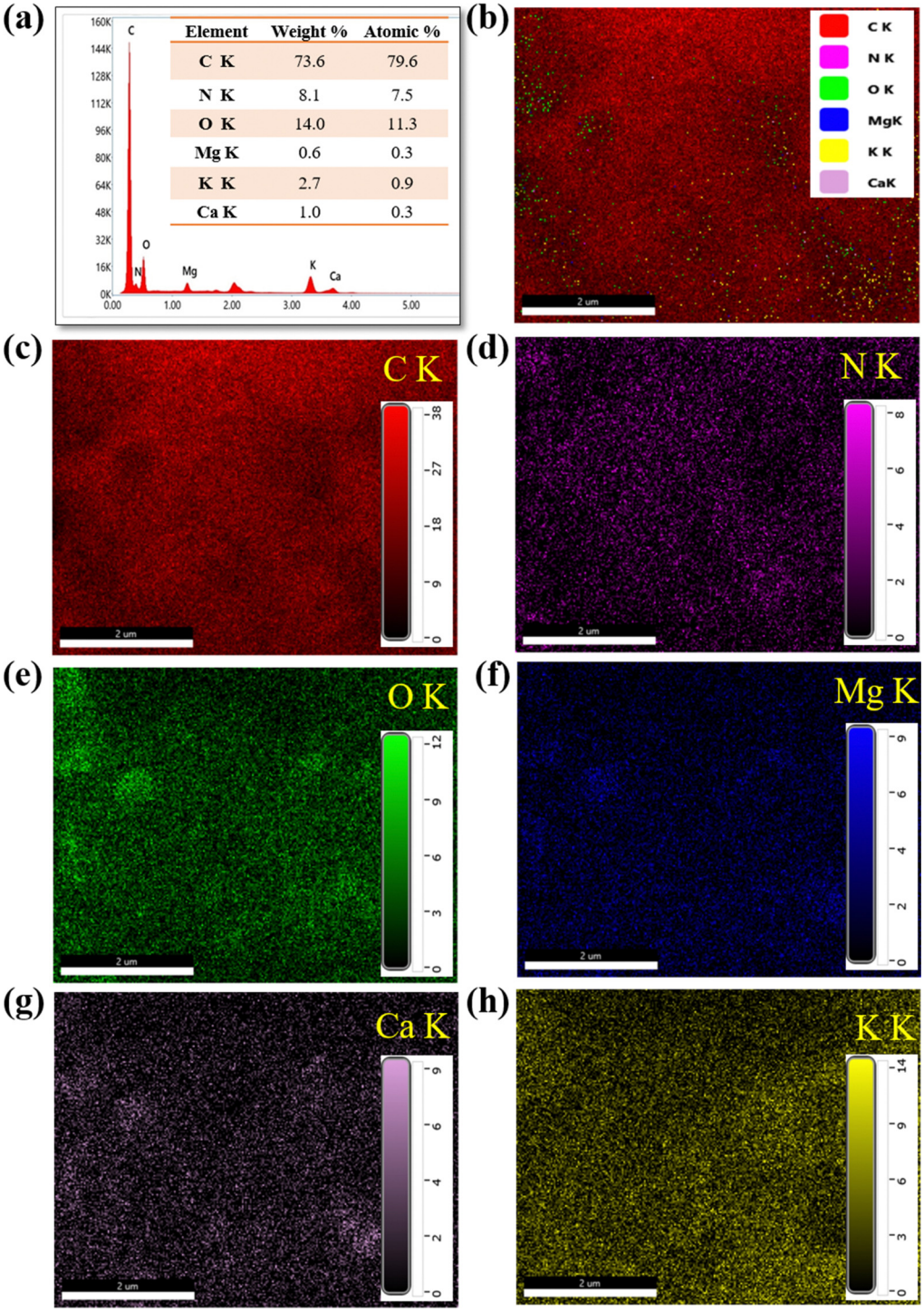

Fig. 4 EDX result with elemental mapping of precarbonized *Z. armatum* derived carbon (PCZ): (a) EDX spectra with elemental composition, and (b)–(h) color mapping of elements.

the hindrance in the flow of electrical current in the electrolytic solution is termed as electrolytic resistance (R_s), resistance of charge transfer (R_{ct}), and double layer capacitance (C).[27–29] On fitting the experimental data using the equivalent circuit model, the sample KZAC showed good charge transfer kinetics with an R_{ct} value of 7.26 Ω. The lower frequency region is less inclined and more diverged from the imaginary *y*-axis with minimal ionic movements ultimately decreasing the capacitance value. The bulk electrolytic resistance for KZAC is found to be 1.25 Ω.

From the Nyquist plot (Fig. 7), it is revealed that the KZAC sample has a somewhat semicircle region indicating a frequency-dependent system. The semicircle region reflects the diffusion of electrolyte into the porous electrode materials.

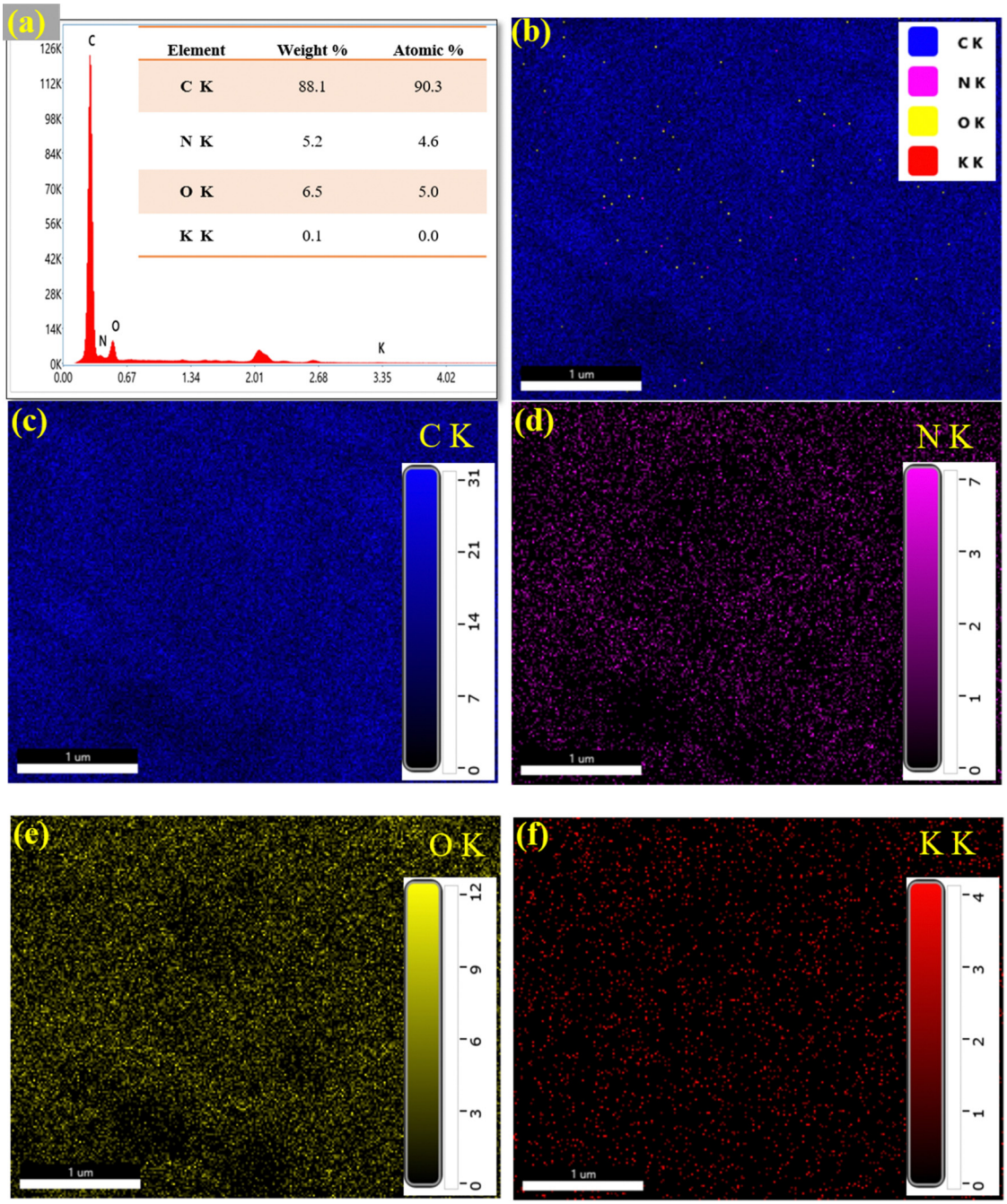

Fig. 5 EDX with color mapping of elements present in *Z. armatum* derived activated carbon (KZAC): (a) EDX spectra with elemental composition, and (b)–(f) color mapping of elements.

From the results, it can be concluded that for the activated carbon derived using KOH, electrolyte (KOH) can easily diffuse within the nanoporous electrode materials. At the lower frequency region, nevertheless, the low frequency region is not vertical and absolutely parallel to the imaginary axis, and the straight line at this region indicates the capacitance behavior of the active materials.

The shift of the lines in the Nyquist plot towards the imaginary axis after 4000 cycles can be attributed to the improved electrode–electrolyte interface development over time. Before cycling, the electrolyte may not be able to completely penetrate the intricate nanoporous carbon structure due to limited contact time.[30] However, during the repeated charging and discharging cycles, the electrolyte has more time to penetrate the complex carbon matrix and establish a better interface with the electrode surface. This gradual development of the electrode–electrolyte interface can lead to the observed shift of the lines towards the imaginary (Z'') axis, reflecting the enhanced capacitive performance of the electrode material.[27,31] Nonetheless, after a certain number of cycles,

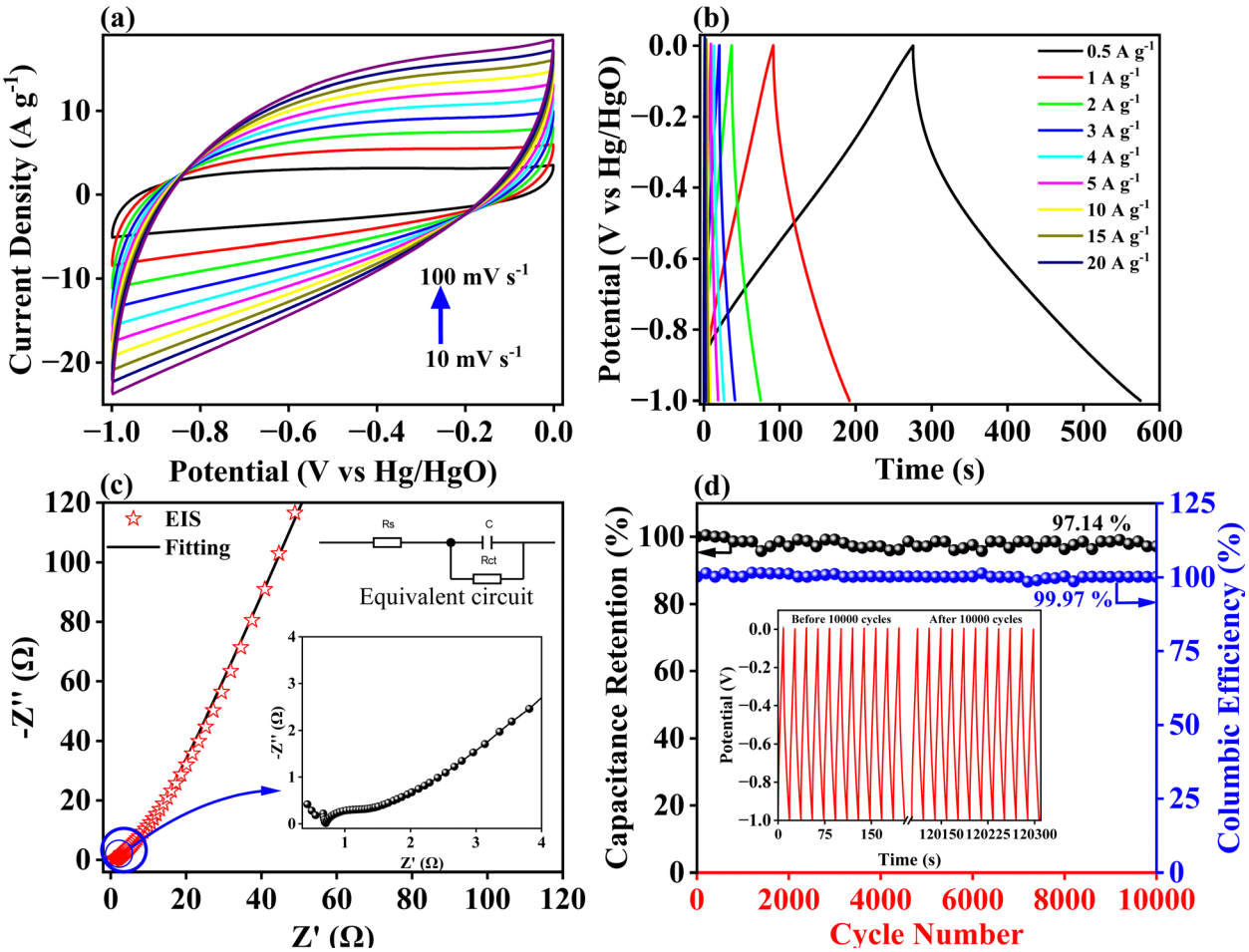

Fig. 6 Electrochemical characterization of the KZAC sample: (a) CV, (b) GCD and (c) Nyquist plot of KZAC and (d) stability and capacitance retention.

the electrode–electrolyte interface becomes fully established and does not undergo further development. At this point, the capacitive performance of the electrode remains constant, as evidenced by the Nyquist plot remaining unchanged in subsequent cycles (Fig. 7).

The electrochemical behaviour of the PCZ sample is depicted in Fig. 8. Fig. 8(a) represents CV at different scan rates from 10 to 100 mV s^{-1}. As compared to the KZAC sample, its area under the CV curve is smaller and hence exhibited lower specific capacitance. The GCD plot as shown in Fig. 8(b) revealed gravimetric capacitance of 14.82, 10.25, 7.62, 4.98, and 2.15 F g^{-1} at a current density of 0.5, 1, 2, 3, and 5 A g^{-1}. The Nyquist plot of the sample showed higher resistive behavior due to its non-porous structure. It possesses lower ionic movement, which results in decreased capacitive value. The charge transfer resistance (R_{ct}) value for PCZ was found to be 9.23 Ω. The higher R_{ct} value for PCZ suggests incomplete carbonization at the lower temperature of 280 °C, potentially hindering the complete opening of all pores and no clear channeling. Conversely, the higher surface areas and pore volumes of the KZAC sample facilitate the efficient diffusion of ions within the interconnected three-dimensional porous network, thereby contributing to enhanced supercapacitive performance.

This study investigates the potential of activated carbon derived from waste *Z. armatum* seeds as an electrode material for electrochemical double-layer capacitors (EDLCs). Compared

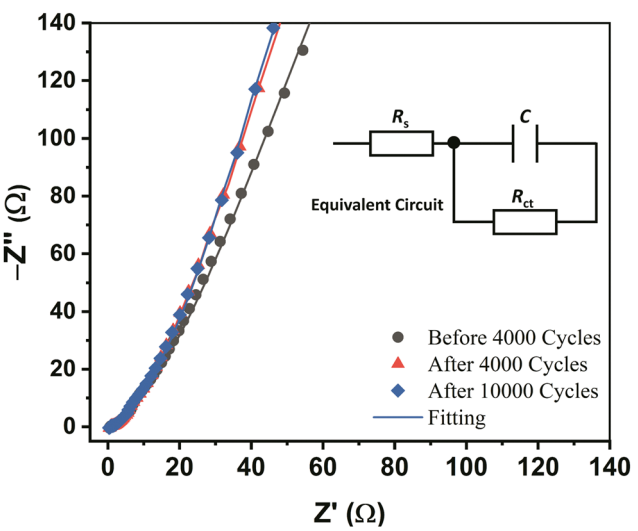

Fig. 7 Nyquist plot of KZAC at different cycles.

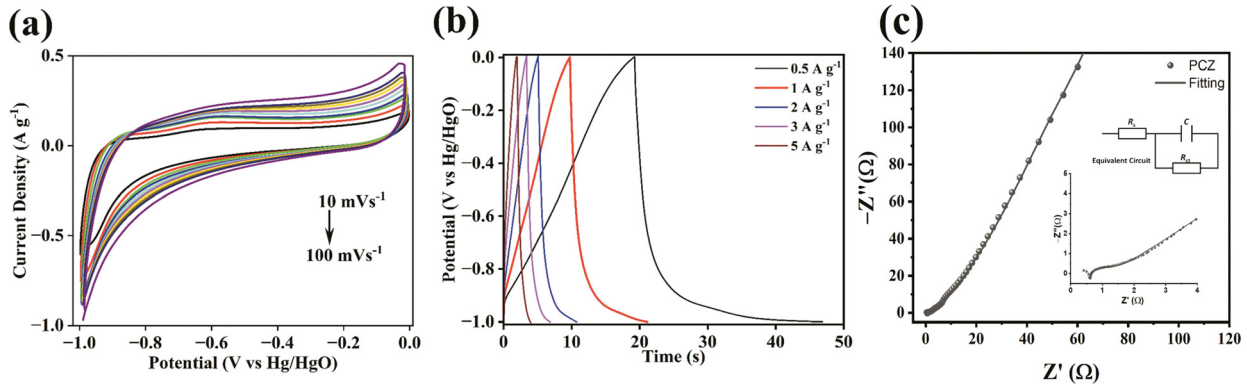

Fig. 8 Electrochemical characterization of the PCZ sample: (a) CV, (b) GCD and (c) Nyquist plot.

Table 1 Comparative overview of the supercapacitive performance of various biomass-derived activated carbons and this work

S. no.	Biomass sources	Activation by	Specific capacitance ($F\ g^{-1}$)	Current density	Capacity retention (cycles)	Electrolytes	Ref.
1	Corn husk	KOH	127	1 A g^{-1}	90% (5000)	6 M KOH	32
2	Areca nut midrib	KOH	154	1 A g^{-1}	—	1 M KOH	33
3	Cherrystones	KOH	120	1 mA cm^{-2}	—	1 M $TEABF_4$/AN	34
4	Pecan nutshell	H_3PO_4	129	5 mV s^{-1}	90% (5000)	1 M CH_3COONa	35
5	Waste sticks/wood	KOH	133	1 A g^{-1}	99% (10 000)	6 M KOH	36
6	Waste coffee powder tea	Melamine + KOH	148	0.5 A g^{-1}	97% (10 000)	3 M KOH	37
7	Waste part of *Z. armatum* seeds	KOH	148.08	0.5 A g^{-1}	97.14% (10 000)	6 M KOH	This work

to other biomass-derived activated carbons, the *Z. armatum* seed-based material exhibits promising characteristics, particularly in terms of capacitance and cyclic retention compared to other biomass derived activated carbon. A detailed comparison of the supercapacitive performance of these materials is presented in Table 1.

4. Conclusions

In this work, activated carbon was prepared using waste chunks of *Z. armatum* seeds, initially by precarbonization followed by carbonization at 900 °C in a tube furnace. A highly porous activated carbon material was found to be prepared with excellent surface area of 554.10 $m^2\ g^{-1}$ of KZAC. The as-prepared AC was characterized and electrochemical assessment was carried out using a three electrode system. The result shows the 148.08 F g^{-1} specific capacitance at 0.5 F g^{-1} current density. Based on the results, the AC could act as a negative electrode in supercapacitor applications. The stability of the material was assessed in terms of electrochemical impedance spectroscopy and galvanostatic charge discharge. All in all, the results show that the prepared activated carbon material is a promising activated carbon for energy storage applications.

Author contributions

Conceptualization: Deval Prasad Bhattarai, Puspa Lal Homagai & Ram Lal Swagat Shrestha, lab work: Deval Prasad Bhattarai, Sabin Aryal, Pawan Kumar Mishra, Timila Shrestha, manuscript preparation: Deval Prasad Bhattarai, Sabin Aryal, Khem Raj Shrestha, Hari Bhakta Oli; review and editing: Deval Prasad Bhattarai, Hari Bhakta Oli, Puspa Lal Homagai, Ram Lal Swagat Shrestha; supervision: Deval Prasad Bhattarai, Puspa Lal Homagai, Ram Lal Shrestha.

Data availability

The data supporting this article have been included as part of the Article.

Conflicts of interest

All authors declare that we have no known competing interests or personal relationships that could have appeared to influence the work reported in this paper.

Acknowledgements

This research was supported by the University Grants Commission, Nepal (Faculty Research Grant: FRG 77/78-S&T-3).

References

1 K. R. Shrestha, S. Kandula, N. H. Kim and J. H. Lee, Core cation tuned $MxCo_{3-x}S_4$@ $NiMoS_4$ [M = Ni, Mn, Zn] core–shell nanomaterials as advanced all solid-state asymmetric

supercapacitor electrodes, *Chem. Eng. J.*, 2021, **405**, 127046, DOI: 10.1016/j.cej.2020.127046.

2 G. P. Awasthi, D. P. Bhattarai, B. Maharjan, K.-S. Kim, C. H. Park and C. S. Kim, Synthesis and characterizations of activated carbon from Wisteria sinensis seeds biomass for energy storage applications, *J. Ind. Eng. Chem.*, 2019, **72**, 265–272, DOI: 10.1016/j.jiec.2018.12.027.

3 R. L. Shrestha, T. Shrestha, B. M. Tamrakar, R. G. Shrestha, S. Maji, K. Ariga and L. K. Shrestha, Nanoporous carbon materials derived from washnut seed with enhanced supercapacitance, *Materials*, 2020, **13**(10), 2371, DOI: 10.3390/ma13102371.

4 S. Kandula, K. R. Shrestha, N. H. Kim and J. H. Lee, Fabrication of a 3D hierarchical sandwich Co9S8/α-MnS@N–C@ MoS2 nanowire architectures as advanced electrode material for high performance hybrid supercapacitors, *Small*, 2018, **14**(23), 1800291, DOI: 10.1002/smll.201800291.

5 J. Deng, T. Xiong, H. Wang, A. Zheng and Y. Wang, Effects of cellulose, hemicellulose, and lignin on the structure and morphology of porous carbons, *ACS Sustainable Chem. Eng.*, 2016, **4**(7), 3750–3756, DOI: 10.1021/acssuschemeng.6b00388.

6 W. Sun, Y. Zhang, Z. Yang and F. Yang, High-performance activated carbons for electrochemical double layer capacitors: Effects of morphology and porous structures, *Int. J. Energy Res.*, 2020, **44**(3), 1930–1950, DOI: 10.1002/er.5047.

7 A. C. Forse, C. Merlet, J. M. Griffin and C. P. Grey, New perspectives on the charging mechanisms of supercapacitors, *J. Am. Chem. Soc.*, 2016, **138**(18), 5731–5744, DOI: 10.1021/jacs.6b02115.

8 P. Simon, Y. Gogotsi and B. Dunn, Where do batteries end and supercapacitors begin?, *Science*, 2014, **343**(6176), 1210–1211, DOI: 10.1126/science.1249625.

9 V. Siipola, T. Tamminen, A. Källi, R. Lahti, H. Romar, K. Rasa, R. Keskinen, J. Hyväluoma, M. Hannula and H. Wikberg, Effects of biomass type, carbonization process, and activation method on the properties of bio-based activated carbons, *BioResources*, 2018, **13**(3), 5976–6002.

10 K. Mensah-Darkwa, C. Zequine, P. K. Kahol and R. K. Gupta, Supercapacitor energy storage device using biowastes: A sustainable approach to green energy, *Sustainability*, 2019, **11**(2), 414, DOI: 10.3390/su11020414.

11 Y. Yang, D. Chen, W. Han, Y. Cheng, B. Sun, C. Hou, G. Zhao, D. Liu, G. Chen and J. Han, Nature-inspired self-activation method for the controllable synthesis of highly porous carbons for high-performance supercapacitors, *Carbon*, 2023, **205**, 1–9, DOI: 10.1016/j.carbon.2023.01.013.

12 S. E. Kayode and F. J. González, Treatment of biowaste for electrodes in energy storage applications: a brief review, *J. Compos. Sci.*, 2023, **7**(3), 127, DOI: 10.3390/jcs7030127.

13 S. Adhikari, K. Subedi, S. Dhungana, R. L. Arhyal, H. Paudyal, K. N. Ghimire, B. R. Poudel and M. R. Pokhrel, Chemical modification of banana peels and banana pseudostem for the adsorptive removal of chromium(VI) from aqueous solution, *J. Nepal Chem. Soc.*, 2023, **43**(2), 23–33, DOI: 10.3126/jncs.v43i2.53338.

14 Y. X. Gan, Activated carbon from biomass sustainable sources, *C-J. Carbon Res.*, 2021, **7**(2), 39, DOI: 10.3390/c7020039.

15 R. Farma, R. I. Julita, I. Apriyani, A. Awitdrus and E. Taer, ZnCl2-assisted synthesis of coffee bean bagasse-based activated carbon as a stable material for high-performance supercapacitors, *Mater. Today: Proc.*, 2023, **87**, 25–31, DOI: 10.1016/j.matpr.2023.01.370.

16 M. Iwanow, T. Gärtner, V. Sieber and B. König, Activated carbon as catalyst support: precursors, preparation, modification and characterization, *Beilstein J. Org. Chem.*, 2020, **16**(1), 1188–1202, DOI: 10.3762/bjoc.16.104.

17 P. Mishra, S. Aryal, H. Oli, T. Shrestha, M. A. Mamun, R. L. Shrestha and D. Bhattarai, Enhanced Energy Storage: Electrochemical Performance of ZnCl2-Activated Carbon Derived from Acacia catechu Bark, *Mong. J. Chem.*, 2024, **25**(52), 26–34.

18 P. Nowicki, I. Kuszyńska, J. Przepiórski and R. Pietrzak, The effect of chemical activation method on properties of activated carbons obtained from pine cones, *Cent. Eur. J. Chem.*, 2013, **11**, 78–85, DOI: 10.2478/s11532-012-0140-0.

19 D. Shrestha and A. Rajbhandari, The effects of different activating agents on the physical and electrochemical properties of activated carbon electrodes fabricated from wood-dust of Shorea robusta, *Heliyon*, 2021, **7**(9), e07917, DOI: 10.1016/j.heliyon.2021.e07917.

20 R. L. Shrestha, R. Chaudhary, T. Shrestha, B. M. Tamrakar, R. G. Shrestha, S. Maji, J. P. Hill, K. Ariga and L. K. Shrestha, Nanoarchitectonics of lotus seed derived nanoporous carbon materials for supercapacitor applications, *Materials*, 2020, **13**(23), 5434, DOI: 10.3390/ma13235434.

21 C.-K. Sim, S. R. Majid and N. Z. Mahmood, Electrochemical performance of activated carbon derived from treated food-waste, *Int. J. Electrochem. Sci.*, 2015, **10**(12), 10157–10172, DOI: 10.1016/s1452-3981(23)11250-8.

22 Y. Nagaraju, H. Ganesh, S. Veeresh, H. Vijeth and H. Devendrappa, A strategy of making waste profitable: Self-templated synthesis of helical rod structured porous carbon derived from Ganoderma Lucidem for advanced supercapacitor electrode, *Diamond Relat. Mater.*, 2023, **131**, 109607, DOI: 10.1016/j.diamond.2022.109607.

23 W. Chen, M. Gong, K. Li, M. Xia, Z. Chen, H. Xiao, Y. Fang, Y. Chen, H. Yang and H. Chen, Insight into KOH activation mechanism during biomass pyrolysis: Chemical reactions between O-containing groups and KOH, *Appl. Energy*, 2020, **278**, 115730, DOI: 10.1016/j.apenergy.2020.115730.

24 A. Pourjavadi, H. Abdolmaleki, M. Doroudian and S. H. Hosseini, Novel synthesis route for preparation of porous nitrogen-doped carbons from lignocellulosic wastes for high performance supercapacitors, *J. Alloys Compd.*, 2020, **827**, 154116, DOI: 10.1016/j.jallcom.2020.154116.

25 Z. Heidarinejad, M. H. Dehghani, M. Heidari, G. Javedan, I. Ali and M. Sillanpää, Methods for preparation and activation of activated carbon: a review, *Environ. Chem. Lett.*, 2020, **18**, 393–415, DOI: 10.1007/s10311-019-00955-0.

26 C. Jin, J. Nai, O. Sheng, H. Yuan, W. Zhang, X. Tao and X. W. D. Lou, Biomass-based materials for green lithium secondary batteries, *Energy Environ. Sci.*, 2021, **14**(3), 1326–1379, DOI: 10.1039/d0ee02848g.

27 S. Aryal, K. R. Shrestha, T. Shrestha, H. B. Oli, I. Pathak, R. L. S. Shrestha and D. P. Bhattarai, Activated Carbon from Prunus persica Seed Stones as a Negatrode Material for High-Performance Supercapacitors, *J. Mol. Struct.*, 2024, **1323**, 140810, DOI: **10.1016/j.molstruc.2024.140810**.

28 P. K. Mishra, K. R. Shrestha, H. B. Oli, T. Shrestha, L. P. Joshi, R. L. S. Shrestha and D. P. Bhattarai, High-performance porous activated carbon derived from Acacia catechu bark as nanoarchitectonics material for supercapacitor applications, *J. Taiwan Inst. Chem. Eng.*, 2024, **165**, 105761, DOI: **10.1016/j.jtice.2024.105761**.

29 M. Dhakal, X. Wei, H. B. Oli, N. Chen, Y. Sun, D. B. Pokharel, Q. Ren, J. Dong and W. Ke, Effects of water content on the corrosion behavior of NiCu low alloy steel embedded in compacted GMZ bentonite, *J. Mater. Sci. Technol.*, 2024, DOI: **10.1016/j.jmst.2024.08.070**.

30 F. Barzegar, D. Y. Momodu, O. O. Fashedemi, A. Bello, J. K. Dangbegnon and N. Manyala, Investigation of different aqueous electrolytes on the electrochemical performance of activated carbon-based supercapacitors, *RSC Adv.*, 2015, **5**(130), 107482–107487, DOI: **10.1039/C5RA21962K**.

31 S. B. Dhavale, V. L. Patil, S. S. Patil, R. P. Dhavale, H.-H. Park, T. Kim and P. S. Patil, Nanostructured NiCo2O4 embedded on biowaste derived hierarchical porous activated carbon for high performance symmetric and asymmetric supercapacitor device, *J. Energy Storage*, 2023, **72**, 108820, DOI: **10.1016/j.est.2023.108820**.

32 M. Usha Rani, K. Nanaji, T. N. Rao and A. S. Deshpande, Corn husk derived activated carbon with enhanced electrochemical performance for high-voltage supercapacitors, *J. Power Sources*, 2020, **471**, 228387, DOI: **10.1016/j.jpowsour.2020.228387**.

33 A. Yunita, R. Farma, A. Awitdrus and I. Apriyani, The effect of various electrolyte solutions on the electrochemical properties of the carbon electrodes of supercapacitor cells based on biomass waste, *Mater. Today: Proc.*, 2023, **87**, 246–252, DOI: **10.1016/j.matpr.2023.03.102**.

34 M. Olivares-Marín, J. A. Fernández, M. J. Lázaro, C. Fernández-González, A. Macías-García, V. Gómez-Serrano, F. Stoeckli and T. Centeno, Cherry stones as precursor of activated carbons for supercapacitors, *Mater. Chem. Phys.*, 2009, **114**(1), 323–327, DOI: **10.1016/j.matchemphys.2008.09.010**.

35 D. Martínez-Casillas, I. Mascorro-Gutiérrez, C. Arreola-Ramos, H. Villafán-Vidales, C. Arancibia-Bulnes, V. Ramos-Sánchez and A. Cuentas-Gallegos, A sustainable approach to produce activated carbons from pecan nutshell waste for environmentally friendly supercapacitors, *Carbon*, 2019, **148**, 403–412, DOI: **10.1016/j.carbon.2019.04.017**.

36 A. R. Selvaraj, D. Chinnadurai, I. Cho, J.-S. Bak and K. Prabakar, Bio-waste wood-derived porous activated carbon with tuned microporosity for high performance supercapacitors, *J. Energy Storage*, 2022, **52**, 104928, DOI: **10.1016/j.est.2022.104928**.

37 J. Choi, C. Zequine, S. Bhoyate, W. Lin, X. Li, P. Kahol and R. Gupta, Waste coffee management: deriving high-performance supercapacitors using nitrogen-doped coffee-derived carbon, *C-J. Carbon Res.*, 2019, **5**(3), 44, DOI: **10.3390/c5030044**.